

Mass Production of Monodisperse Carbon Microspheres with Size-Dependent Supercapacitor Performance via Aqueous Self-Catalyzed Polymerization

Qiang Yu,^[a] Doudou Guan,^[a] Zechao Zhuang,^[a] Jiantao Li,^[a] Changwei Shi,^[a] Wen Luo,^[a] Liang Zhou,^{*,[a]} Dongyuan Zhao,^[a] and Liqiang Mai^{*,[a, b]}

A facile, aqueous, self-catalyzed polymerization method has been developed for the mass production of monodisperse phenolic resin and carbon microspheres. The synthesis is mainly based on the self-catalyzed reaction between phenol derivatives and the hydrolysis products of hexamethylenetetramine (HMTA). The obtained phenolic resin spheres have a tunable size of 0.8–6.0 μm , depending on the type of phenol and HMTA/phenol ratio. Treating the phenolic resin with steam at an elevated temperature results in monodisperse carbon microspheres with abundant micropores, high surface area, and

rich surface functionality. The resultant carbon spheres exhibit a size-dependent electrical double-layer capacitor performance; the capacitance increases with decreasing particle size. The nitrogen and oxygen codoped carbon spheres with the smallest size (≈ 600 nm) deliver a high specific capacitance (282 F g^{-1} at 0.5 A g^{-1}), excellent rate capability (170 F g^{-1} at 20 A g^{-1}), and outstanding cycling stability (95.3% capacitance retention after 10000 cycles at 5 A g^{-1}). This study provides a new avenue for the mass production of monodisperse carbon microspheres.

Introduction

Monodisperse carbon spheres integrate the unique advantages of both porous carbon materials and spherical colloids into one entity; this endows them with indispensable applications in water purification, catalysis, drug delivery, as well as energy storage and conversion.^[1–7] The carbonization of polymer spheres has been demonstrated to be an effective approach for the preparation of carbon spheres. However, the most intensively studied polymer spheres, such as polystyrene (PS) and poly(methyl methacrylate) (PMMA), cannot be converted into their carbon analogous, owing to their poor thermal stability.^[8,9]


Phenolic resin spheres are excellent precursors for the production of carbon spheres. Dong et al. reported the preparation of polymer and carbon nanospheres through the polymerization of resorcinol and formaldehyde by using L-lysine as the catalyst.^[10] Zhao and co-workers developed a low-concentration hydrothermal route for the synthesis of highly uniform, ordered, mesoporous carbon spheres by using phenol–formaldehyde

resol as the precursor and triblock copolymer as the soft template.^[11] Inspired by the synthesis of Stöber silica spheres, Lu and co-workers reported the synthesis of monodisperse phenolic resin and carbon spheres through the polymerization of resorcinol and formaldehyde in a mixture of ammonia–ethanol–water.^[12] These seminal studies create tremendous opportunities for the design of monodisperse carbon-based spheres, such as microporous carbon,^[9,13–15] mesoporous carbon,^[16–23] graphitic carbon,^[24] hollow carbon,^[25–30] and yolk–shell carbon spheres.^[31–35] However, all of these approaches involve the employment of ammonia, ethanol, hydrofluoric acid, and/or hydrothermal treatment in autoclaves at a high temperature during the synthesis, which makes scaled-up production challenging.

Herein, we report a facile aqueous method for the mass production of monodisperse phenolic resin and the corresponding carbon microspheres through the self-catalyzed polymerization of phenol derivatives and the hydrolysis products of hexamethylenetetramine (HMTA). A series of phenols, such as 3-aminophenol, 2-aminophenol, 4-aminophenol, and resorcinol, can be employed as the precursors. The as-obtained phenolic resin spheres have a tunable size of 0.8–6.0 μm , depending on the synthetic conditions. Treating the phenolic resin spheres with steam at an elevated temperature generates carbon spheres with slightly reduced size (0.6–5.0 μm), high specific surface area ($836 \text{ m}^2 \text{ g}^{-1}$), and rich surface functionality (N and O codoping). When used as the electrode materials for electrical double-layer capacitors (EDLCs), the carbon spheres exhibit a size-dependent electrochemical performance; the specific capacitance increases with decreasing particle size. The nitrogen and oxygen codoped carbon microspheres derived from 3-ami-

[a] Q. Yu, D. Guan, Z. Zhuang, J. Li, C. Shi, W. Luo, Prof. L. Zhou, Prof. D. Zhao, Prof. L. Mai
State Key Laboratory of Advanced Technology for
Materials Synthesis and Processing
International School of Materials Science and Engineering
Wuhan University of Technology, Wuhan 430070 (P.R. China)
E-mail: liangzhou@whut.edu.cn
mlq518@whut.edu.cn

[b] Prof. L. Mai
Department of Chemistry
University of California
Berkeley, CA 94720 (USA)

 The ORCID identification number(s) for the author(s) of this article can be found under <https://doi.org/10.1002/cplu.201700182>.

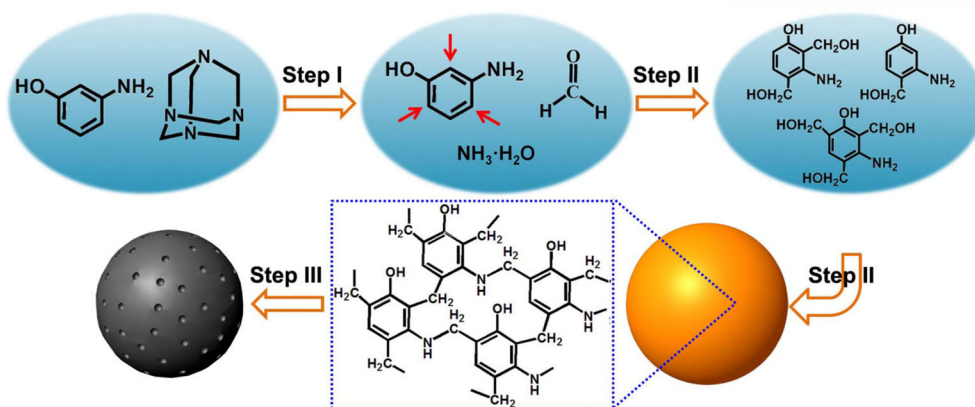


Figure 1. Schematic illustration for the formation of phenolic resin and carbon microspheres. Step I: the hydrolysis of HMTA; step II: polymerization between 3-aminophenol and formaldehyde; step III: carbonization.

nophenol–formaldehyde exhibit a high specific capacitance of 282 Fg^{-1} . Excellent rate capability (170 Fg^{-1} at 20 Ag^{-1}) and outstanding cycling stability (95.3% capacitance retention after 10 000 cycles at 5 Ag^{-1}) has also been demonstrated.

Results and Discussion

Figure 1 shows a schematic illustration for the preparation of phenolic resin and carbon microspheres. A phenol derivative (such as 3-aminophenol) and HMTA, two cheap and widely available chemicals, are employed as the only precursors. HMTA, which is frequently used curing agent in phenolic resin production, hydrolyzes under mild conditions, generating formaldehyde and ammonia (Figure 1, step I). Ammonia, in turn, catalyzes the polymerization of phenol derivatives and formaldehyde, which results in the formation of phenolic resin spheres (Figure 1, step II). The amino group on 3-aminophenol can also catalyze the polymerization reaction. Considering the fact that polymerization between 3-aminophenol and formaldehyde is catalyzed by ammonia generated from HMTA and the amino group, the synthetic process is termed self-catalyzed polymerization. Treatment of the phenolic resin spheres with steam at an elevated temperature converts the polymer spheres into microporous carbon spheres (Figure 1, step III). Apart from 3-aminophenol, 2-aminophenol, 4-aminophenol, and resorcinol can also be used as the precursors for the production of phenolic resin and carbon microspheres. The yields of the phenolic resin and carbon spheres reach as high as 29.9 and 15.9 gL^{-1} , respectively (Figure S1 in the Supporting Information).

Figure 2 shows the SEM and TEM images of typical 3-aminophenol–formaldehyde resin (PF-1) and the corresponding carbon (PFC-1) microspheres. (See the Experimental Section for an explanation of sample labels.) PF-1 has a monodisperse spherical morphology with a smooth surface; the size of the resin spheres are determined to be approximately $0.89 \mu\text{m}$ (Figure 2a,b). The FTIR spectrum (Figure S2 in the Supporting Information) clearly shows the stretching/deformation vibrations of $-\text{OH}$ ($\tilde{\nu} \approx 3357 \text{ cm}^{-1}$), $-\text{NH}$ ($\tilde{\nu} \approx 3357 \text{ cm}^{-1}$), $\text{C}-\text{N}$ ($\tilde{\nu} \approx 1202$ and 1239 cm^{-1}), $\text{C}-\text{O}$ ($\tilde{\nu} \approx 1363 \text{ cm}^{-1}$), $\text{C}=\text{C}$ ($\tilde{\nu} \approx 1622$

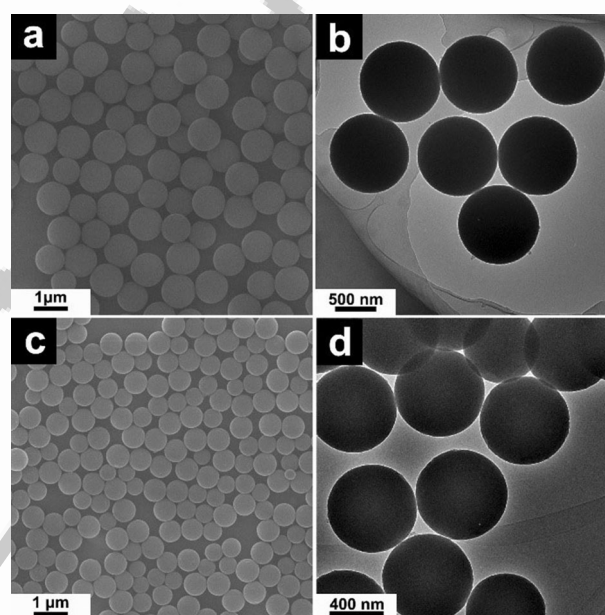


Figure 2. SEM (a,c) and TEM (b,d) images of PF-1 (a,b) and PFC-1 (c,d). $[\text{HMTA}]/[\text{3-aminophenol}] = 16$.

and 1507 cm^{-1}), and $-\text{CH}_2$ ($\tilde{\nu} \approx 2927 \text{ cm}^{-1}$); this confirms the proposed structure of the phenolic resin, as shown in Figure 1. Carbonization of PF-1 in a flow of $\text{H}_2\text{O}/\text{N}_2$ at 800°C produces nitrogen and oxygen codoped carbon (PFC-1).

The obtained PFC-1 (Figure 2c,d) inherits the uniform spherical morphology of the parent resin; this demonstrates that the phenolic resin is an ideal precursor for producing carbon materials. The size of the microspheres shrinks from approximately $0.89 \mu\text{m}$ for PF-1 to approximately $0.60 \mu\text{m}$ for PFC-1 during the carbonization process, which corresponds to a 32% shrinkage in diameter. No graphitic structure can be observed in the high-magnification TEM image, which suggests the amorphous nature of PFC-1 (Figure S3 in the Supporting Information).

The amorphous feature of PFC-1 is further confirmed by wide-angle XRD and Raman spectroscopy. The XRD pattern of PFC-1 (Figure S4 in the Supporting Information) manifests two broad diffraction peaks at $2\theta = 24$ and 43° , which are charac-

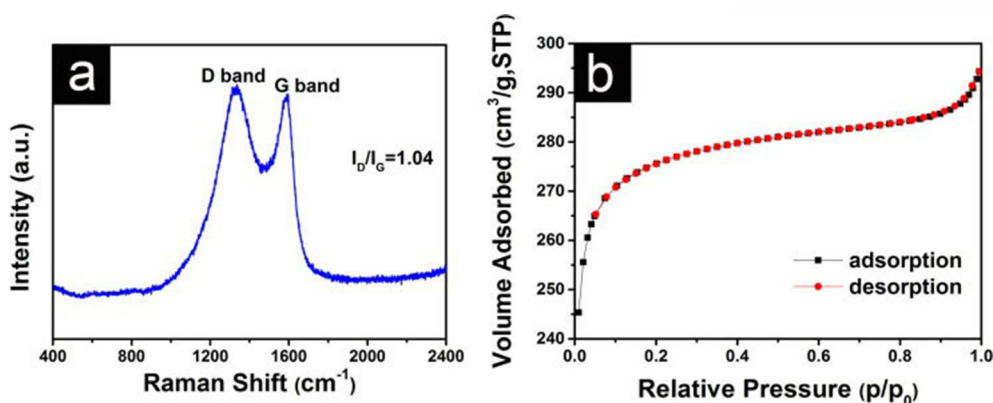


Figure 3. Raman spectrum (a) and nitrogen adsorption/desorption isotherms (b) of PFC-1. [HMTA]/[3-aminophenol] = 16.

teristic for amorphous carbon. The Raman spectrum of PFC-1 (Figure 3a) features a broad band at $\tilde{\nu} \approx 1340 \text{ cm}^{-1}$ (D band), together with a relatively narrow band at $\tilde{\nu} \approx 1585 \text{ cm}^{-1}$ (G band). The G band is associated with graphitic sp^2 -bonded carbon, whereas the D band corresponds to disordered carbon or defective graphitic structures. The comparable intensities of the D and G bands ($I_D/I_G = 1.04$) indicate that the as-prepared carbon materials are generally amorphous.

Nitrogen adsorption-desorption measurements were performed to investigate the pore structure of the carbon microspheres. PFC-1 manifests a typical type I isotherm (Figure 3b), which reveals the microporous structure. From the nitrogen adsorption-desorption isotherm, the microporous surface area, BET surface area, microporous volume, and total pore volume of PFC-1 are determined to be $772 \text{ m}^2 \text{ g}^{-1}$, $836 \text{ m}^2 \text{ g}^{-1}$, $0.40 \text{ cm}^3 \text{ g}^{-1}$, and $0.46 \text{ cm}^3 \text{ g}^{-1}$, respectively. The rich micro-

porosity and high specific surface area of the PFC materials are essential for EDLC applications.

For comparison, the specific surface areas and pore volumes of PF-1 and the sample prepared without steam (PFC-1') are also provided (Figure S5 and Table S2 in the Supporting Information). PF-1 shows a very low surface area of $7 \text{ m}^2 \text{ g}^{-1}$, and sample PFC-1' manifests a moderate surface area of $422 \text{ m}^2 \text{ g}^{-1}$. These results suggest that steam functions as an activation agent during carbonization. The possible reactions between carbon and steam at elevated temperatures include $\text{C} + \text{H}_2\text{O} \rightarrow \text{CO} + \text{H}_2$ and $\text{C} + 2\text{H}_2\text{O} \rightarrow \text{CO}_2 + 2\text{H}_2$. By etching off a small fraction of carbon atoms, carbon microspheres with a high specific surface area and rich microporosity could be obtained.

The surface composition of the PFC microspheres were studied by X-ray photoelectron spectroscopy (XPS). The survey spectrum (Figure 4a) shows that the surface of PFC-1 is com-

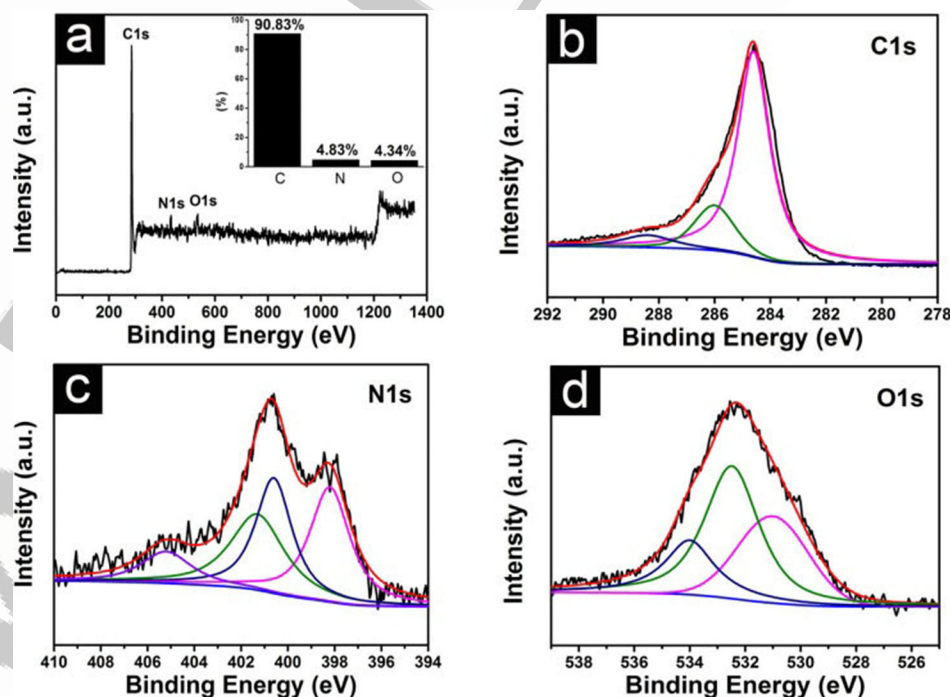


Figure 4. XPS survey spectrum (a) and high-resolution C 1s (b), N 1s (c), and O 1s (d) spectra of PFC-1.

posed of carbon (90.83%), nitrogen (4.83%), and oxygen (4.34%); this suggests the successful incorporation of nitrogen and oxygen heteroatoms. The high-resolution C 1s core level XPS spectrum (Figure 4b) can be deconvoluted into three components: sp^2 -bonded C at 284.6 eV (75.53%), C in C–O and C–N bonds at 285.9 eV (17.33%), and C in C=O bonds at 288.4 eV (7.14%).^[21] The N 1s core level spectrum (Figure 4c) suggests the presence of four types of nitrogen: pyridinic N located at 398.2 eV (36.34%), pyrrolic N at 400.6 eV (24.64%), quaternary N at 401.4 eV (33.16%), and pyridine N–O moieties at 405.2 eV (5.86%).^[15] According to previous reports, pyridinic and pyrrolic nitrogen are electrochemically active and can contribute to the pseudocapacitance.^[15,36] Moreover, quaternary nitrogen incorporated into the graphitic carbon plane can significantly enhance the electrical conductivity of the carbon materials.^[36] The O 1s spectrum (Figure 4d) shows three types of oxygen functionalities: isolated carbonyl groups (C=O) at 531.1 eV, carbonyl groups in carboxyl at 532.5 eV, and oxygen

singly bonded in phenols (C–OH) or ethers (C–O–C) at 534.0 eV.^[37]

To investigate the effects of synthetic parameters on the structure of the resin and carbon spheres, the molar ratio of HMTA/3-aminophenol (R) was systematically tuned from 1 to 16. With an R value of 1, the obtained PF-6 shows a uniform spherical morphology with a mean size of 1.97 μm . By adjusting the R value from 1 to 16, the size of the PF spheres decreases monotonously from 1.97 to 0.89 μm (Figure 5). After carbonization, all samples kept the original spherical structure (Figure 6a–e). As in the case of PF spheres, the size of the carbon spheres decreases with increasing R value; with R increasing from 1 to 16, the particle size decreases from 1.53 to 0.60 μm (Figure 6). The phenomenon that the particle size of resin and carbon spheres decreases with R value can be explained as follows. With an increase of R value, the concentration of HMTA also increases, while the concentration of 3-aminophenol remains constant (Table S1 in the Supporting Infor-

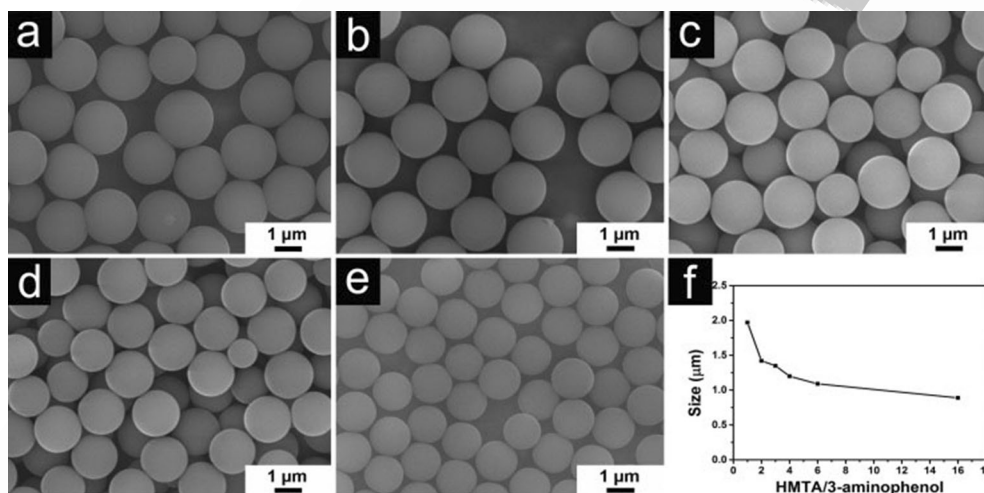


Figure 5. SEM images of the PF resin spheres prepared with R values of 1 (a, PF-6), 2 (b, PF-5), 3 (c, PF-4), 4 (d, PF-3), and 6 (e, PF-2). f) Particle size of the PF spheres as a function of R value.

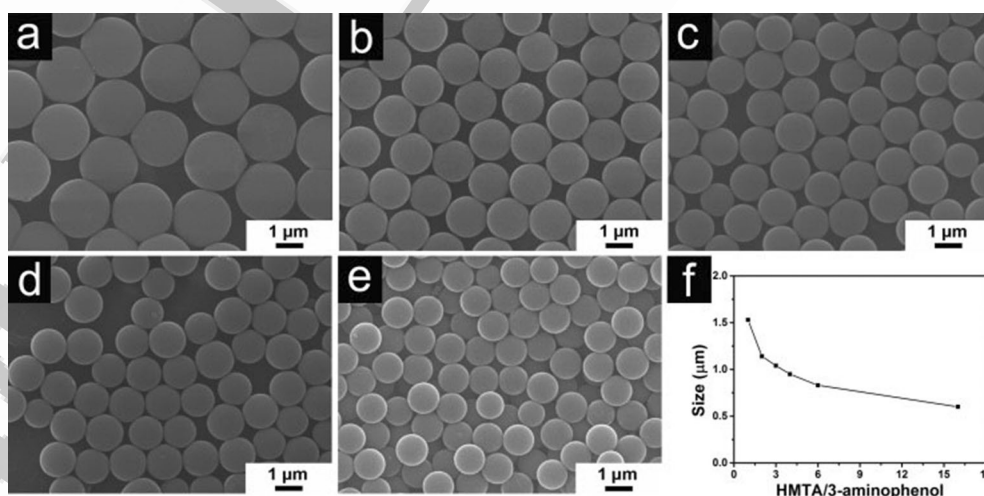


Figure 6. SEM images of the PFC spheres prepared with R values of 1 (a, PFC-6), 2 (b, PFC-5), 3 (c, PFC-4), 4 (d, PFC-3), and 6 (e, PFC-2). f) Particle size of the PFC spheres as a function of R value.

mation). The hydrolysis of HMTA releases ammonia and formaldehyde. Ammonia, in turn, catalyzes the polymerization of 3-aminophenol and formaldehyde. At high ammonia and formaldehyde concentrations, a large number of nuclei are generated, which consequently lead to a small size.

Apart from 3-aminophenol, other phenol derivatives, such as 2-aminophenol, 4-aminophenol, and resorcinol, can also be used as the precursors to prepare resin and carbon spheres. However, 2- and 4-aminophenol only lead to polydisperse PF spheres (Figure S6 in the Supporting Information), which is in good agreement with a report in the literature.^[9] When resorcinol is used as the precursor, larger PF spheres (PF-11) with sizes up to 5.72 μm can be obtained (Figure S7a in the Supporting Information). Carbonization of the PF-11 spheres reduces the size from 5.72 to 4.60 μm (Figure S7b in the Supporting Information). It should be mentioned that the sizes of PF-11 and PFC-11 are much larger than those obtained in most previous reports based on a modified Stöber method.^[9,12,15,38,39] The above results unambiguously demonstrate that the aqueous self-catalyzed reaction route developed herein is quite versatile, and it can be applied to the preparation of phenolic resin and carbon spheres with various diameters and functionalities.

Interestingly, a significant amount of nitrogen can be observed in the PF spheres, even if the phenol derivative contains no nitrogen. For example, PF-9, which is prepared from resorcinol, contains a high nitrogen content of 11.2% (Figure S8 in the Supporting Information); this suggests the incorporation of NH_4^+ released from HMTA into the PF polymer. Owing to

the contribution from NH_4^+ , the nitrogen content generally increases with the HMTA/3-aminophenol ratio. PFC-1, PFC-3, and PFC-5 have nitrogen contents of 4.83, 4.01, and 3.85%, respectively (Figure S9 and Table S3 in the Supporting Information).

Considering the high surface area, rich microporosity, and moderate nitrogen and oxygen contents of the products, the PFC spheres were studied as electrode materials for EDLCs. The EDLC performance is monitored with a three-electrode configuration in 6.0 M aqueous solutions of KOH. To ensure full penetration of the electrolyte into the microporous network, the as-prepared electrode slices are soaked in the electrolyte solution for 12 h. Figure 7a shows the cyclic voltammetry (CV) profiles of the PFC-1 spheres at scan rates of 5–100 mV s^{-1} . PFC-1 exhibits quasi-rectangular shaped CV curves, even at a high sweep rate of 100 mV s^{-1} , which indicates the very fast electrochemical response and ideal EDLC behavior. Typical galvanostatic charge–discharge curves of PFC-1 are presented in Figure 7b. The charge–discharge profiles are quasi-isosceles triangular in shape, which further confirms the excellent capacitive behavior. The specific capacitances are calculated from the discharge curves. PFC-1 delivers high specific capacitances of 282 and 170 F g^{-1} at current densities of 0.5 and 20 A g^{-1} , respectively; this corresponds to a capacitance retention of 60%. For comparison, the rate performances of PFC-1, PFC-3, and PFC-5 are summarized in Figure 7c. The PFC spheres show size-dependent electrochemical performances. The specific capacitance increases with decreasing particle size. PFC-1, with a diameter of 0.60 μm , delivers the highest specific capacitance. The superior EDLC performance of PFC-1 can be attrib-

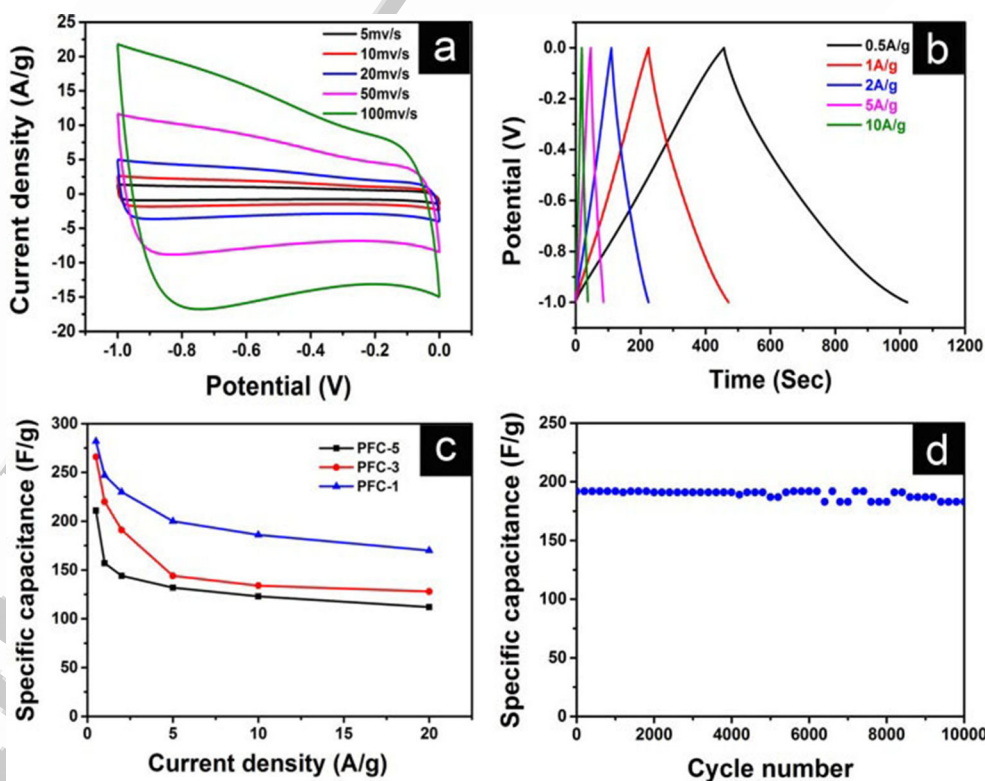


Figure 7. EDLC performance of PFC-1 in 6.0 M KOH: a) CV profiles of PFC-1 at various sweep rates; b) galvanostatic charge/discharge curves of PFC-1 recorded at various current densities; c) rate performance of PFC-1 ([HMTA]/[3-aminophenol] = 16), PFC-3 ([HMTA]/[3-aminophenol] = 4), and PFC-5 ([HMTA]/[3-aminophenol] = 2); d) cycling stability of PFC-1 at a current density of 5 A g^{-1} .

uted to it having the smallest size and highest specific surface area (Figure S10 and Table S2 in the Supporting Information). To further investigate the cycling stability, 10 000 consecutive charge–discharge cycles were recorded for PFC-1 at a current density of 5 Ag^{-1} (Figure 7d). Remarkably, over 95.3% of the capacitance can be retained after 10 000 cycles, which suggests the outstanding cycling stability.

The superior EDLC performance of PFC-1 can be ascribed to the following structural features. 1) PFC-1 possesses rich microporosity and a high specific surface area, which are beneficial for capacitive charge storage.^[40] 2) It contains a considerable amount of nitrogen and oxygen functionalities, which improve the wettability of carbon towards electrolytes.^[9,41,42] With enhanced surface wettability, the electrolyte ions are able to penetrate into the micropores of PFC-1 smoothly, which results in high surface utilization for electrical-double layer formation. 3) The successful incorporation of nitrogen and oxygen functionalities bring extra sites for reversible redox reactions, providing pseudocapacitance to the overall capacitance of the material.^[43,44] The pseudocapacitance contribution can be evidenced from the high specific capacitance per surface area ($33.6 \mu\text{F cm}^{-2}$), which is much higher than the experimental and theoretical upper limit of specific double-layer capacitance per surface area ($15\text{--}20 \mu\text{F cm}^{-2}$).^[42] 4) Nitrogen doping also enhances the conductivity of the materials, which is beneficial for the rate capability.^[45]

The aqueous self-catalyzed polymerization approach developed herein has the following attractive features. 1) Both precursors, phenol derivatives and HMTA, are very cheap and widely available. 2) Unlike modified Stöber methods, water is used as the solvent rather than a mixture of water–ethanol, which significantly lowers the synthetic costs. 3) Unlike modified Stöber methods, no ammonia is used in the synthesis. Instead, ammonia released from the hydrolysis of HMTA and the amino group on aminophenol catalyze the polymerization of phenol derivatives and formaldehyde. 4) The yields of phenolic resin and carbon microspheres are fairly high, reaching 29.9 (theoretical value = 30.5 g L^{-1} , according to Table S1 in the Supporting Information) and 15.9 g L^{-1} , respectively. 5) The obtained phenolic resin and carbon microspheres are highly monodisperse. The abovementioned features make the aqueous self-catalyzed polymerization approach feasible for mass production.

Conclusion

We have demonstrated a facile, aqueous, self-catalyzed polymerization method for the mass production of monodisperse phenolic resin and carbon microspheres. The yields of resin and carbon spheres reached 29.9 and 15.9 g L^{-1} , respectively. In particular, this methodology allows the production of carbon microspheres with rich microporosity (microporous volume = $0.40 \text{ cm}^3 \text{ g}^{-1}$, microporous surface area = $772 \text{ m}^2 \text{ g}^{-1}$), high surface area ($840 \text{ m}^2 \text{ g}^{-1}$), well-controlled surface functionality (N and O codoping), and tunable size ($0.60\text{--}4.60 \mu\text{m}$). These unique structural features result in excellent electrochemical performances in EDLCs. As-obtained nitrogen and

oxygen codoped PFC-1 delivered a high specific capacitance (282 F g^{-1} at 0.5 Ag^{-1}), excellent rate capability (170 F g^{-1} at 20 Ag^{-1}), and outstanding cycling stability (95.3% capacitance retention after 10 000 cycles at 5 Ag^{-1}). This study provides a new avenue for the mass production of monodisperse porous carbon spheres with a broad range of potential applications.

Experimental Section

Preparation of phenolic resin and carbon microspheres

The phenolic resin spheres were synthesized through the polymerization of phenol derivatives and the hydrolysis products of HMTA ($\text{C}_6\text{H}_{12}\text{N}_4$). In a typical synthesis, 3-aminophenol (0.5 g) and HMTA (0.64 g) were dissolved in deionized water (20 mL) and stirred for 20 min. After dissolution, the solution was heated to 85°C and kept at that temperature for 24 h under constant stirring. The resin spheres were collected by centrifugation, washed with water (3 \times), and dried at 70°C . To obtain the carbon spheres, the resin spheres were heated to 800°C at a heating rate of 2°C min^{-1} and kept at 800°C for 5 h, during which $\text{H}_2\text{O}/\text{N}_2$ was continuously passed through the quartz tube. To study the effects of synthetic conditions, the HMTA/phenol ratio (R) was tuned from 0.5 to 16, and 3-aminophenol was substituted by 2-aminophenol, 4-aminophenol, and resorcinol (Table S1 in the Supporting Information). The resultant resin and carbon microspheres were denoted as PF- x and PFC- x , in which PF is the abbreviation for phenol–formaldehyde, PFC is the abbreviation for phenol–formaldehyde-derived carbon, and x is the sample number.

Characterization

Field-emission SEM images were collected on a JEOL-7100F scanning electron microscope at 20 KV. TEM images were collected on a JEM-2100F microscope at 200 KV. The BET surface areas and pore size distributions were calculated from the nitrogen sorption results, which were measured on a Tristar-3020 instrument at 77 K. Before the measurements, the samples were degassed at 200°C for 5 h. XPS analysis was conducted on a VG Multilab 2000 instrument. FTIR spectroscopy was performed by using a Nexus, America Thermo Nicolet, spectrometer.

Electrochemical measurements

Prior to the electrochemical tests, the nickel foam was ultrasonically cleaned in acetone, ethanol, and deionized water, successively. Electrochemical measurements were performed on an CHI 760D electrochemical workstation with a three-electrode configuration. The working electrodes were prepared by mixing 80 wt% PFC, 10 wt% polytetrafluoroethylene, and 10 wt% carbon black. The mass loading of the active material was approximately $3\text{--}4 \text{ mg cm}^{-2}$. A 6.0 M aqueous solution of KOH was used as the electrolyte. Platinum wire and a saturated calomel electrode were used as the counter and reference electrodes, respectively.

Acknowledgements

This study was supported by the National Key Research and development program of China (2016YFA0202603), the National Basic Research Program of China (2013CB934103), the National

Natural Science Foundation of China (51521001, 51502226, 21673171), the Programme of Introducing Talents of Discipline to Universities (B17034), the National Natural Science Fund for Distinguished Young Scholars (51425204), and the Fundamental Research, Funds for the Central Universities (201611001, 201611002). L.M. gratefully acknowledges financial support from the China Scholarship Council (no. 201606955096).

Conflict of interest

The authors declare no conflict of interest.

Keywords: carbon · doping · electrochemistry · microporous materials · polymers

- [1] J. Liu, N. P. Wickramaratne, S. Qiao, M. Jaroniec, *Nat. Mater.* **2015**, *14*, 763–774.
- [2] P. Zhang, Z. Qiao, S. Dai, *Chem. Commun.* **2015**, *51*, 9246–9256.
- [3] X. Sun, Y. Li, *Angew. Chem. Int. Ed.* **2004**, *43*, 597–601; *Angew. Chem.* **2004**, *116*, 607–611.
- [4] F. Xu, Z. Tang, S. Huang, L. Chen, Y. R. Liang, W. Mai, H. Zhong, R. Fu, D. Wu, *Nat. Commun.* **2015**, *6*, 7221.
- [5] J. Zhou, J. Lian, L. Hou, J. Zhang, H. Gou, M. Xia, M. Zhao, T. Strobel, L. Tao, F. Gao, *Nat. Commun.* **2015**, *6*, 8563. ■ ■ incorrect authors for this article no., please check ■ ■.
- [6] B. Friedel, S. Greulich-Weber, *Small* **2006**, *2*, 859–863.
- [7] L.-Q. Mai, A. Minhas-Khan, X. Tian, K. M. Hercule, Y.-L. Zhao, L. Xu, X. Xu, *Nat. Commun.* **2013**, *4*, 2923.
- [8] A. Lu, G. Hao, Q. Sun, *Angew. Chem. Int. Ed.* **2011**, *50*, 9023–9025; *Angew. Chem.* **2011**, *123*, 9187–9189.
- [9] J. Zhao, W. Niu, L. Zhang, H. Cai, M. Han, Y. Yuan, S. Majeed, S. Anjum, G. Xu, *Macromolecules* **2013**, *46*, 140–145.
- [10] Y. Dong, N. Nishiyama, Y. Egashira, K. Ueyama, *Ind. Eng. Chem. Res.* **2008**, *47*, 4712–4716.
- [11] Y. Fang, D. Gu, Y. Zou, Z. Wu, F. Li, R. Che, Y. Deng, B. Tu, D. Zhao, *Angew. Chem. Int. Ed.* **2010**, *49*, 7987–7991; *Angew. Chem.* **2010**, *122*, 8159–8163.
- [12] J. Liu, S. Qiao, H. Liu, J. Chen, A. Orpe, D. Zhao, G. Lu, *Angew. Chem. Int. Ed.* **2011**, *50*, 5947–5951; *Angew. Chem.* **2011**, *123*, 6069–6073.
- [13] S. Wang, W. Li, G. Hao, Y. Hao, Q. Sun, X. Zhang, A. Lu, *J. Am. Chem. Soc.* **2011**, *133*, 15304–15307.
- [14] Z. Xu, Q. Guo, *Carbon* **2013**, *52*, 464–467.
- [15] N. Wickramaratne, J. Xu, M. Wang, L. Zhu, L. Dai, M. Jaroniec, *Chem. Mater.* **2014**, *26*, 2820–2828.
- [16] J. Choma, D. Jamiola, K. Augustynek, M. Marszewski, M. Gao, M. Jaroniec, *J. Mater. Chem.* **2012**, *22*, 12636–12642.
- [17] J. Liu, T. Yang, D. Wang, G. Lu, D. Zhao, S. Qiao, *Nat. Commun.* **2013**, *4*, 94–105. ■ ■ incorrect article no., please check ■ ■.
- [18] Y. Fang, G. Zheng, J. Yang, H. Tang, Y. Zhang, B. Kong, Y. Lv, C. Xu, A. Asiri, J. Zhang, D. Zhao, *Angew. Chem. Int. Ed.* **2014**, *53*, 5366–5370; *Angew. Chem.* **2014**, *126*, 5470–5474.
- [19] Y. Fang, Y. Lv, F. Gong, Z. Wu, X. Li, H. Zhu, L. Zhou, C. Yao, F. Zhang, G. Zheng, D. Zhao, *J. Am. Chem. Soc.* **2015**, *137*, 2808–2811.
- [20] J. Tang, J. Liu, C. Li, Y. Li, M. Tade, S. Dai, Y. Yamauchi, *Angew. Chem. Int. Ed.* **2015**, *54*, 588–593; *Angew. Chem.* **2015**, *127*, 598–603.
- [21] J. Wang, H. Liu, J. Diao, X. Gu, H. H. Wang, J. F. Rong, B. Zong, D. Su, *J. Mater. Chem. A* **2015**, *3*, 2305–2313.
- [22] C. Liu, M. Yu, Y. Li, J. S. Li, J. Wang, C. Yu, L. Wang, *Nanoscale* **2015**, *7*, 11580–11590.
- [23] J. Hou, T. Cao, F. Idrees, C. Cao, *Nanoscale* **2016**, *8*, 451–457.
- [24] K. Ai, Y. Liu, C. Ruan, L. Lu, G. Lu, *Adv. Mater.* **2013**, *25*, 998–1003.
- [25] A. Fuertes, P. Valle-Vigon, M. Sevilla, *Chem. Commun.* **2012**, *48*, 6124–6126.
- [26] T. Yang, J. Liu, R. Zhou, Z. Chen, H. Xu, S. Qiao, M. Monteiro, *J. Mater. Chem. A* **2014**, *2*, 18139–18146.
- [27] H. Zhang, M. Yu, H. Song, O. Noonan, J. Zhang, Y. Yang, L. Zhou, C. Yu, *Chem. Mater.* **2015**, *27*, 6297–6304.
- [28] H. Zhang, O. Noonan, X. Huang, Y. Yang, C. Xu, L. Zhou, C. Yu, *ACS Nano* **2016**, *10*, 4579–4586.
- [29] C. Liu, J. Wang, J. Li, R. Luo, J. Shen, X. Sun, W. Han, L. Wang, *ACS Appl. Mater. Interfaces* **2015**, *7*, 18609–18617.
- [30] C. Liu, J. Wang, J. Li, M. Zeng, R. Luo, J. Shen, X. Sun, W. Han, L. Wang, *ACS Appl. Mater. Interfaces* **2016**, *8*, 7194–7204.
- [31] X. Zhang, Y. Li, C. Cao, *J. Mater. Chem.* **2012**, *22*, 13918–13921.
- [32] Z. Qiao, B. Guo, A. Binder, J. Chen, G. Veith, S. Dai, *Nano Lett.* **2013**, *13*, 207–212.
- [33] Q. Sun, B. He, X. Zhang, A. Lu, *ACS Nano* **2015**, *9*, 8504–8513.
- [34] T. Yang, R. Zhou, D. Wang, S. Jiang, Y. Yamauchi, S. Qiao, M. Monteiro, J. Liu, *Chem. Commun.* **2015**, *51*, 2518–2521.
- [35] J. Wang, S. Feng, Y. Song, W. Li, W. Gao, A. Elzatahry, D. Aldhayan, Y. Xia, D. Zhao, *Catal. Today* **2015**, *243*, 199–208.
- [36] Q. Wang, J. Yan, Z. Fan, *Energy Environ. Sci.* **2016**, *9*, 729–762.
- [37] A. Olejniczak, M. Leżańska, A. Pacuła, P. Nowak, J. Włoch, J. Łukasiewicz, *Carbon* **2015**, *91*, 200–214.
- [38] S. Tanaka, H. Nakao, T. Mukai, Y. Katayama, Y. Miyake, *J. Phys. Chem. C* **2012**, *116*, 26791–26799.
- [39] H. Zhou, S. Xu, H. Su, M. Wang, W. Qiao, L. Ling, D. Long, *Chem. Commun.* **2013**, *49*, 3763.
- [40] D. Wang, F. Li, M. Liu, G. Lu, H. Cheng, *Angew. Chem. Int. Ed.* **2008**, *47*, 373–376; *Angew. Chem.* **2008**, *120*, 379–382.
- [41] G. Shen, X. Sun, H. Zhang, Y. Liu, J. Zhang, A. Meka, L. Zhou, C. Z. Yu, *J. Mater. Chem. A* **2015**, *3*, 24041–24048.
- [42] G. Hasegawa, T. Deguchi, K. Kanamori, Y. Kobayashi, H. Kageyama, T. Abe, K. Nakanishi, *Chem. Mater.* **2015**, *27*, 4703–4712.
- [43] T. Lin, I. Chen, F. Liu, C. Yang, H. Bi, F. Xu, F. Huang, *Science* **2015**, *350*, 1508–1513.
- [44] W. Shen, W. Fan, *J. Mater. Chem. A* **2013**, *1*, 999–1013.
- [45] H. Chen, F. Sun, J. Wang, W. Li, W. Qiao, L. Ling, D. Long, *J. Phys. Chem. C* **2013**, *117*, 8318–8328.

Manuscript received: April 10, 2017

Revised manuscript received: May 23, 2017

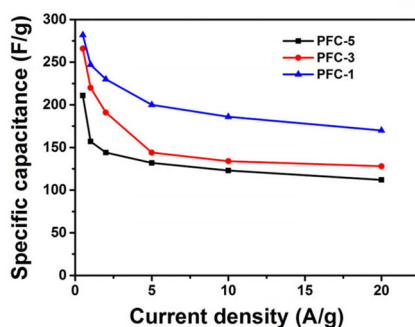
Accepted manuscript online: May 31, 2017

Version of record online: ■ ■ ■ 0000

FULL PAPERS

Q. Yu, D. Guan, Z. Zhuang, J. Li, C. Shi,
W. Luo, L. Zhou,* D. Zhao, L. Mai*

■■■ - ■■■
**Mass Production of Monodisperse
Carbon Microspheres with Size-
Dependent Supercapacitor
Performance via Aqueous Self-
Catalyzed Polymerization**



Size versus capacitance: A facile, aqueous, self-catalyzed polymerization method has been developed for the mass production of monodisperse carbon microspheres. The resultant carbon spheres exhibit a size-dependent supercapacitor performance; the capacitance increases with decreasing particle size. Nitrogen and oxygen codoped carbon spheres deliver a high specific capacitance, excellent rate capability, and outstanding cycling stability (see figure). ■■■ graphic was cropped ■■■



Self-catalyzed #polymerization produces #carbonmicrospheres with size-dependent #supercapacitance @UC-Berkeley [SPACE RESERVED FOR IMAGE AND LINK](#)

Share your work on social media! *ChemPlusChem* has added Twitter as a means to promote your article. Twitter is an online microblogging service that enables its users to send and read text-based messages of up to 140 characters, known as “tweets”. Please check the pre-written tweet in the galley proofs for accuracy. Should you or your institute have a Twitter account, please let us know the appropriate username (i.e., @accountname), and we will do our best to include this information in the tweet. This tweet will be posted to the journal’s Twitter account @ChemPlusChem (follow us!) upon online publication of your article, and we recommended you to repost (“retweet”) it to alert other researchers about your publication.

Please check that the ORCID identifiers listed below are correct. We encourage all authors to provide an ORCID identifier for each coauthor. ORCID is a registry that provides researchers with a unique digital identifier. Some funding agencies recommend or even require the inclusion of ORCID IDs in all published articles, and authors should consult their funding agency guidelines for details. Registration is easy and free; for further information, see <http://orcid.org/>.

Qiang Yu
Doudou Guan
Zechao Zhuang
Jiantao Li
Changwei Shi
Wen Luo
Prof. Liang Zhou
Prof. Dongyuan Zhao
Prof. Liqiang Mai <http://orcid.org/0000-0003-4259-7725>